

Experimental Observation of an Extremely Dark Material Made By a Low-Density Nanotube Array

Zu-Po Yang,[†] Lijie Ci,[#] James A. Bur,[†] Shawn-Yu Lin,^{*,†} and Pulickel M. Ajayan[#]

The Future Chips Constellation & Department of Physics, Applied Physics and Astronomy, and Department of Material Science and Engineering, Rensselaer Polytechnic Institute, Troy, New York 12180

Received September 14, 2007; Revised Manuscript Received December 9, 2007

ABSTRACT

An ideal black material absorbs light perfectly at all angles and over all wavelengths. Here, we show that low-density vertically aligned carbon nanotube arrays can be engineered to have an extremely low index of refraction, as predicted recently by theory [Garcia-Vidal, F. J.; Pitarke, J. M.; Pendry, J. B. *Phys. Rev. Lett.* 1997, 78, 4289–4292] and, combined with the nanoscale surface roughness of the arrays, can produce a near-perfect optical absorption material. An ultralow diffused reflectance of 1×10^{-7} measured from such arrays is an order-of-magnitude lower compared to commercial low-reflectance standard carbon. The corresponding integrated total reflectance of 0.045% from the nanotube arrays is three times lower than the lowest-ever reported values of optical reflectance from any material, making it the darkest man-made material ever.

An ideal black object absorbs all of the colors of light and reflects none of them. The concept of a perfect absorber has led to the introduction of a blackbody cavity and a successful formulation of the Kirchhoff's law and Planck's radiation law over a century ago.^{1,2} However, the experimental realization of a truly black object has been hindered by our inability to reduce an object's index of refraction to unity and thus eliminate its optical reflection entirely. For example, conventional black paint and graphite absorb visible light strongly due to the π band's optical transition,³ yet they are limited by a moderate reflection of 5–10% at the air–dielectric interface. Recently, a theoretical calculation predicted an extremely low index of refraction ($n = 1.01–1.10$) using a new concept of low-density carbon nanotube array.⁴ Such a nanotube array not only reflects light weakly but also absorbs light strongly.^{3,5} These combined features make it an ideal candidate for realizing a super black object. An ultralow reflectance can also be achieved by random surface scattering.^{6–9} Theoretical modeling of several types of surface diffusers has predicted a low reflectance and a modified reflection pattern.¹⁰ So far, a surface-modified NiP material has been reported to have the lowest reflectance of $R = 0.16–0.18\%$ at normal incidence.^{6,7} However, at a larger angle, $\theta = 60^\circ$, its total reflectance becomes significantly

larger, $R = 4–5\%$, due possibly to its finite etch depth and micrometer size features. To our knowledge, the experimental observations of an extremely low reflectance of $R = 0.01–0.10\%$ and high absorption of $A = 99.9–99.99\%$ using the newly proposed low-density concept are still lacking.

The key to achieve a super low reflectance is to introduce long and low-density nanostructures, which when assembled in ordered arrays, could have deep pores, such as is the case with vertically aligned carbon nanotubes (VA-CNT). Our multiwalled (thin-walled, with very few walls) nanotube samples have a typical tube diameter of 8–11 nm, and the nanotubes are well-aligned with each other. We find that the aligned nanotubes can exhibit a high absorption constant and, more importantly, an extremely low refractive index at visible wavelengths. The aligned nanotube sample, from our observations, makes the best candidate for an ideal super black absorber. The unique conductivities of nanotubes¹¹ are derived from their topology, and small dimensions and are responsible for their optical properties.¹² Additionally, aligned nanotube arrays can be birefringent,³ reflecting differently for different light polarizations⁵ and showing strong light absorption.^{13,14}

The vertically aligned nanotube films were prepared by a water-assisted chemical vapor deposition (CVD) process similar to what has been reported in the literature^{15,16} but yielding few walled nanotubes. The VA-CNT films (ordered arrays comprising a very low density of nanotubes: $0.01–0.02 \text{ g/cm}^3$) can have film thicknesses varied in the range of

* To whom correspondence should be addressed. Telephone: (518)-276-2978. Fax: (518)-276-8042. E-mail: sylin@rpi.edu.

[†] The Future Chips Constellation & Department of Physics, Applied Physics and Astronomy.

[#]Department of Material Science and Engineering.

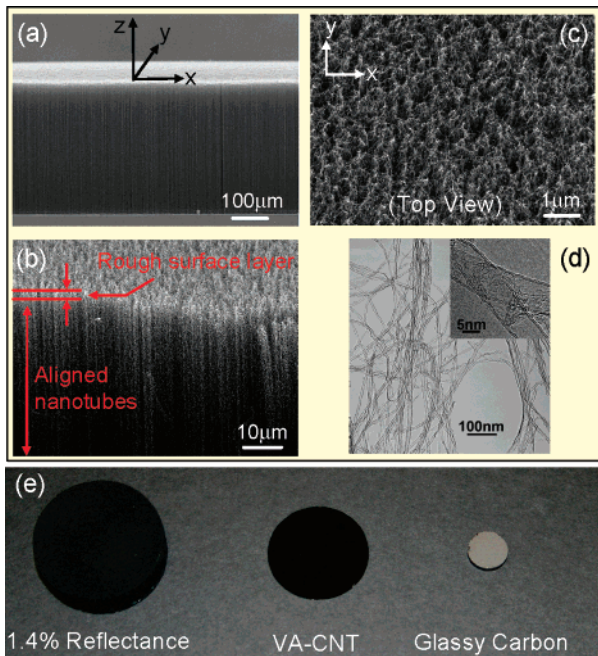


Figure 1. (a) Scanning electron micrograph (SEM) of a vertically aligned carbon nanotube (CNT) sample. (b) A side-view SEM image of the same sample at a higher magnification. The nanotubes are vertically aligned, forming a highly porous nanostructure. (c) A top-view SEM image of the sample. The nanotubes are entangled with each other, forming a loosely connected random surface. The surface corrugation is on the order of 100–1000 nm. (d) A transmission electron micrograph of the sample, indicating that most of the nanotubes are multiwalled with a diameter $d \sim 10$ nm. (e) A photograph of a 1.4% NIST reflectance standard, a CNT sample, and a piece of glassy carbon, taken under a flash light illumination.

10–800 μm depending on growth time. Once grown on a substrate, these nanotube films can be peeled off to get self-standing films. The volume-filling fraction (f.f.) of the array (based on the diameter and pitch of individual nanotubes in the arrays) offers a new mechanism for tailoring the refractive index of the nanotube film.

Figure 1a shows a scanning electron microscopy (SEM) image of our nanotube film with a 100 μm scale bar. The film is uniform over the entire sample at this length scale. A side-view SEM image of the same sample is shown in Figure 1b, with a scale bar of 10 μm . The nanotubes are straight and vertically aligned except at the sample surface. These aligned nanotubes form a low-density porous nanostructure. In Figure 1c, we show a top-view image of the sample with a scale bar of 1 μm . The top layer exhibits a randomly oriented surface structure with a surface corrugation of about 100–1000 nm. The nanotubes are entangled with each other, forming a loosely connected network. These submicrometer surfaces are unique as they do not form continuous surfaces, and their surface-normal is not well-defined. The diameter distribution of nanotubes using transmission electron microscopy (TEM) reveals (Figure 1d) that the average diameter is 8–10 nm. It will be shown that it is the combination of the low-density array, the nanometer-size nanotubes, and the random surface profile that makes this sample an ideal black object.

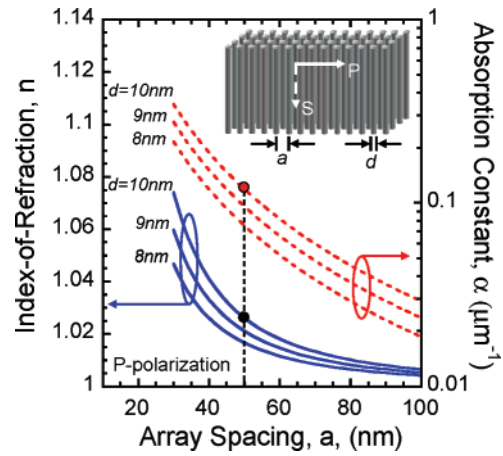


Figure 2. The calculated effective index of refraction and the absorption constant plotted as a function of nanotube spacing. A schematic of the nanotube array and the s and p light polarizations is shown in the inset. For our sample at p polarization, $a = 50$ nm, and $d = 10$ nm, we obtain $n_{\text{effective}}^p = 1.026$ and $\alpha_{\text{effective}}^p = 0.12 \mu\text{m}^{-1}$. This index value is extremely close to unity and could lead to an extremely low optical reflection of $R^p = 0.02\%$.

We now demonstrate the modification of visible light reflection by the nanotube array, and more importantly, we show that we can achieve a super low reflection and super black material with a total reflectance of $R = 0.045\%$. In Figure 1e, we illustrate the qualitative degree of blackness by showing pictures of selective black objects taken by a high-resolution camera. The left-most picture is from a standard reflectance sample certified by the National Institute of Standards and Technology (NIST). Its reflectance is 1.4% at $\lambda = 450\text{--}700$ nm wavelengths. The right-most picture is from a glassy carbon sample. It does not look as dark as the 1.4% reflectance standard. Glassy carbon resembles a black glass¹⁷ and is commonly used as a high-absorbance standard for absorbance calibration. The middle picture is taken from one of our nanotube samples. Due to the use of a flash, these pictures appear brighter than the actual samples when they are viewed under normal illumination. However, our nanotube looks super black compared to the other two conventional black standard objects. Another distinctive feature of these black objects is that they have diffuse optical reflection. Part of the light is scattered by the rough surface into all directions, resulting in a diffuse reflection. This observation prompted us to carry out a systematic study of optical reflection from our nanotube samples.

The optical properties of a carbon nanotube array have been formulated recently using an effective medium theory.⁴ It is found that the dielectric array can be regarded as a composite material and described by an effective index of refraction, $n_{\text{effective}}$. Particularly, it is concluded that the Maxwell–Garnett (MG) approximation holds when the filling fraction f.f. of the array is small, that is, in the low-density limit. As the carbon nanotube is made of shells of graphite, which is birefringent, the effective index of refraction is polarization-dependent. In the inset of Figure 2, we show a schematic of a nanotube array and the corresponding s and p light polarizations. For our nanotube array, it has an average array spacing of $a = (50 \pm 10)$ nm,

a nanotube diameter of $d = 8\text{--}10$ nm, and a filling fraction of f.f. $\approx (2\text{--}3)\%$. Therefore, the MG mean field theory applies. In Figure 2, the computed effective index of refraction and absorption constant⁴ are shown as blue and red curves, respectively. The individual nanotube is assumed to have the dielectric function of graphite.¹⁸ At $a = 50$ nm and $d = 10$ nm, we obtain an $n_{\text{effective}}^p = 1.026$ and an absorption constant $\alpha_{\text{effective}}^p = 0.12 \mu\text{m}^{-1}$ for the p polarization. This index value is extremely close to unity and could lead to an extremely low optical reflection of $R^p = 0.02\%$. We have also computed dielectric properties for the s polarization and found $n_{\text{effective}}^s = 1.074$, $\alpha_{\text{effective}}^s = 2.9 \mu\text{m}^{-1}$, and $R^s = 0.60\%$. For a perfectly aligned array and for the normal incident of light, it is expected that the optical reflection of the array is dominated by the p polarization. Thus, the independence control of the parameters, a and d , of a nanotube array offers new degrees of freedom to realize a super low index of refraction.

To characterize the optical reflection of our samples, we used two complementary experimental setups—one for measuring the total reflectance and the other for testing diffuse reflectance. To obtain the total reflectance, a commercially available integrating sphere was used to perform signal integration over 4π angles. A schematic of it is shown in Figure 3a. Several visible lasers were used for the testing, including $\lambda = 633$ nm from a He–Ne laser and the $\lambda = 514, 488,$ and 458 nm from an Ar laser. The sample is mounted at the center of the sphere, and the incident angle is varied by rotating the sample mount. The reflected light from the sample is uniformly redistributed by the integrating sphere and is collected by a silicon photodetector. Proper black shielding and optical alignment are implemented to prevent leakage of stray light into the integrating sphere. A standard normalization procedure is used to obtain an accurate reflectance. First, the reflecting power from a 99.0% standard is measured and recorded (reference signal). Second, the reflecting power is measured and normalized to the reference signal.

The measured total reflectance (R_{total}) at $\lambda = 633$ nm is shown in Figure 3b. The normal incident data at $\theta_{\text{inc}} = 0^\circ$ will be discussed next and the θ_{inc} -dependence data will be discussed later. First, the measured reflectance of the Au mirror is $R_{\text{total}} = 94.5\%$, which agrees well with the calculated value of $R_{\text{total}} = 94.1\%$. The measured reflectance of the reference sample is $R_{\text{total}} = 1.6\%$, which also agrees with its NIST-certified value of $R_{\text{total}} = 1.4\%$. By this careful calibrating in both the high- and low-reflectance regimes, our measurement accuracy is assured. Second, a glassy carbon is conventionally regarded as a black object and has a measured reflectance of $R_{\text{total}} = 8.5\%$ (the blue dots). Finally, the reflectance of our nanotube array is $R_{\text{total}} = 0.045\%$. The calculated reflectance values from the MG approximation are $R^p = 0.02\%$ and $R^s = 0.6\%$ for p and s polarizations, respectively. If one assumes that the measured reflectance can be approximated by $R_{\text{total}} = fR^p + (1 - f)R^s$, we obtain $f = 95\%$. This would indicate that 95% of the reflectance come from the p polarization and the other 5% from the s polarization. This mixture of polarization may be

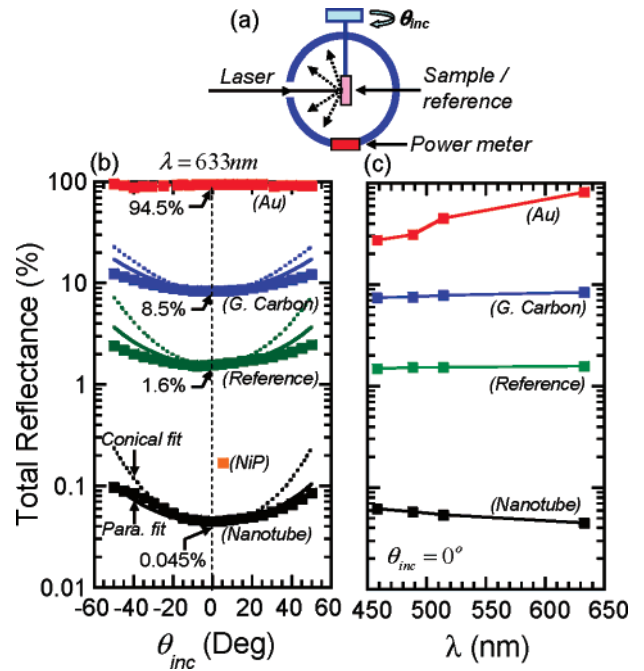


Figure 3. (a) A schematic of the total reflectance measurement setup. The scattered light from the sample under test is uniformly redistributed by the integrating sphere and detected by a power meter. (b) A plot of total reflectance as a function of θ_{inc} . At $\theta_{\text{inc}} = 0^\circ$, the R_{total} is 94.5, 8.5, 1.6, and 0.045% for the Au mirror, the Glassy carbon, the reference, and a nanotube array sample, respectively. The total reflectance of our nanotube array is $R_{\text{total}} = 0.045\%$, 2 orders of magnitude lower than that of the glassy carbon (a conventional black standard). It is also three times lower than the previously reported lowest reflectance of $R_{\text{total}} = 0.16\text{--}0.18\%$,^{6,7} making this nanotube array the darkest man-made material ever. The dashed and solid lines are least-square fits assuming conical and paraboloidal surface profiles, respectively. (c) A plot of total reflectance as a function of visible wavelength, $\lambda = 457\text{--}633$ nm. Both the glassy carbon and the NIST-certified reference exhibit a weak λ dependence. The total reflectance of our nanotube array increases slightly from 0.045 to 0.07% as λ is decreased from 633 to 457 nm.

due to the slightly tilted nanotube array. Nonetheless, the reflectance of our nanotube array is two orders-of-magnitude lower than that of the glassy carbon. This is a remarkable observation because both samples are made up of the same element, carbon. This reflectance value is also three times lower than the previously reported lowest reflectance of $R_{\text{total}} = 0.16\text{--}0.18\%$,^{6,7} making our nanotube array the darkest man-made material ever.

We have also extended our measurement over a broad range of visible wavelengths at $\lambda = 457\text{--}633$ nm, and the results are summarized in Figure 3c. The diffuse Au sample has a lower reflectance at shorter wavelengths due to a stronger material absorption.¹⁸ Both the glassy carbon and the 1.4% reference sample exhibit a weak λ dependence. The total reflectance of our nanotube array increases slightly from 0.045 to 0.07% as λ is decreased from 633 to 457 nm. Hence, the nanotube array maintains an extremely low reflectance throughout the entire range of visible wavelengths. From the conservation of energy, we expect the total incident energy to be transmitted, reflected, or absorbed, that is, $1 = T + R + A$. Thus, a super black material must satisfy the condition

of $R \cong 0$, $T \cong 0$, and $A \cong 1$. We have attempted to measure the transmission intensity of our nanotube array. However, the transmittance is so low that the detected signal is below the noise level of our detector. The upper limit of our nanotube array transmittance is $T \leq 0.001\%$. Hence, a near-perfect absorption of $A = 1 - R - T \cong 99.95\%$ from our nanotube array is demonstrated. We note that a low transmission and a strong absorption is consistent with the calculation result presented Figure 2. The nanotube sample has a $\alpha_{\text{effective}}^{\text{p}} = 0.12 \mu\text{m}^{-1}$ and an absorption length $1/\alpha_{\text{effective}}^{\text{p}} = 8.3 \mu\text{m}$, which is thinner than the $300 \mu\text{m}$ film thickness of our nanotube sample. However, the extremely low n and high absorption can only be partial causes for the observed low reflectance as diffuse scattering by the rough nanotube surface must also play an important role.¹⁰

We now discuss our diffuse reflectance measurement of the samples. This measurement is prompted by two observations. First, the SEM image, shown in Figure 1c, shows the existence of a random surface near the top of our nanotube array. Second, the photo of our nanotube in Figure 1e shows a diffuse reflectance that may be correlated to random surface scattering. Therefore, the diffuse optical scattering from the random surface and its impact on the observed total reflectance must be considered.

A schematic of the angular measurement setup is shown in the inset of Figure 4. Laser light ($\lambda = 633 \text{ nm}$) is incident at an angle, θ_{inc} , from the surface-normal and is detected at a different angle, θ . The laser is polarized perpendicular to the plane defined by the incident light and the sample's surface-normal. The incident power is fixed at 10 mW and is stable to within 2%. For reflection power detection, we use a calibrated silicon photodetector with a detecting area of $(10 \times 10) \text{ mm}^2$ and a corresponding collecting solid angle of $\Delta\Omega = 8.2 \times 10^{-4}$ steradian. Due to the large dynamic range of the reflectance power, we have also checked our detector's linearity from 10 mW to 1 nW. The noise level of the silicon photodetector is 0.05 nW at room temperature.

The measured diffuse reflectance is presented in Figure 4 as a semilogarithmic plot over 8 orders of magnitude. For comparison purposes, we again tested a series of samples that include a Au mirror, a diffuse Au, a glassy carbon, a graphite, and a nanotube sample. All measurements were taken at $\theta_{\text{inc}} = 0^\circ$, except for the Au mirror where $\theta_{\text{inc}} = -10^\circ$. For the Au mirror, its reflectance has a peak value of 94.5% at $\theta = +10^\circ$ and decreases quickly to below $R \approx 10^{-6}$ for $|\theta_{\text{inc}}| \geq 40^\circ$. This is a characteristic of specular reflection from an optically smooth reflecting surface. Diffuse Au is also a good reflector, yet it scatters light into random directions. The measured reflectance exhibits a cosine dependence (the black dashed line) on θ and has a maximum value, $R \cong 2 \times 10^{-4}$, at $|\theta| \leq 5^\circ$. This dependence is known as the idealized Lambertian distribution of a randomly scattered light.^{10,19} Glassy carbon and graphite also exhibit a Lambertian-like dependence but have a lower reflectance of $R \cong 2 \times 10^{-5}$ at $|\theta| \leq 5^\circ$. This reflectance value is 10 times lower than that of diffused Au and is conventionally viewed as a black object. The much lower reflectance is due

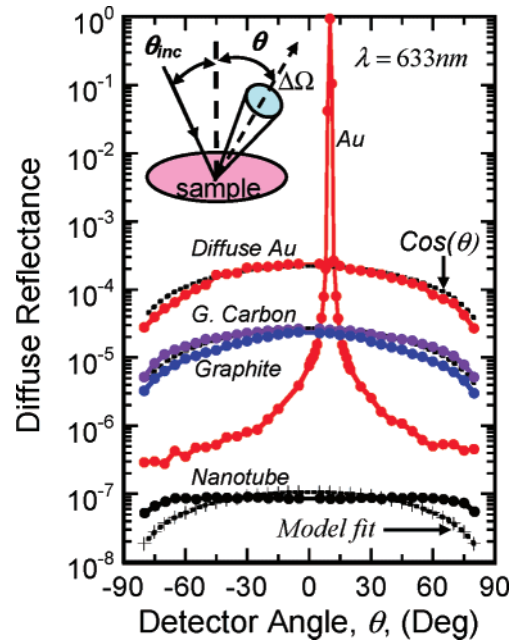


Figure 4. The measured diffuse reflectance data are plotted versus θ over 8 orders of magnitude. A schematic of the diffuse reflectance test setup is shown in the inset. The Au mirror exhibits specular reflection with a strong reflection peak of 94.5%. The reflectance of diffuse Au exhibits a cosine functional dependence (the black dashed line), a characteristic of the so-called “Lambertian distribution.” The graphite and glassy samples also exhibit a Lambertian-like distribution, but their reflectance is about 10 times weaker. The reflection from our CNT sample does not have an observable θ dependence for $|\theta| \leq 70^\circ$. More strikingly, it exhibits a super low diffuse reflectance of $R \cong 1 \times 10^{-7}$ for $|\theta| \leq 70^\circ$, 2 orders of magnitude lower than conventional black objects such as the graphite or glassy carbon. The laser light is incident at an angle θ_{inc} away from the surface-normal and is detected by a photodetector over a range of angles, θ .

to a combination of a small refractive index of the carbon-based material ($n = 1.7\text{--}2$ at $\lambda = 400\text{--}700 \text{ nm}$), the material's absorption,³ and the random scattering of light. Finally, the nanotube array shows a nearly θ -independent reflection pattern and a diffuse reflectance of $R \cong 1 \times 10^{-7}$ for $|\theta| \leq 70^\circ$. This reflectance is extremely low. It is 2 orders of magnitude lower than that of either graphite or a glassy carbon and 7 orders lower than that of the Au mirror. The angular independence together with the ultralow reflectance suggests that our nanotube array is a strong diffuser. The phenomena of such a low reflectance ($R \cong 1 \times 10^{-7}$) and the absence of angular dependence up to $|\theta| \leq 70^\circ$ for a nanotube structure have not been observed experimentally or predicted theoretically.

The observed diffused reflection over a large dynamic range shown in Figure 4 suggests the importance of the effect of surface roughness. In general, a rough surface can be characterized by the root-mean-square of the diffuser height σ_{rms} and the correlation length w of the rough surface. A strong surface corrugation gives a large σ_{rms} and, hence, a large phase delay, $S = 4\pi(\sigma_{\text{rms}}/\lambda) \cos \theta_{\text{inc}}$, for the reflected light.^{10,21–22} The specific radiation pattern from a rough surface can be modeled if the roughness profile is known.^{10,19–22} Recognizing that our nanotube array is a strong

diffuser and also the need for a model that predicts reflectance over a large dynamic range, a model by Shirley and George was chosen.¹⁰ In their model, two types of surface profiles, conical and paraboloidal, are analyzed and their far-field radiation patterns predicted. For the conical profile, the correlation function is cone-shaped near the origin, and the reflectance pattern depends on a single parameter, $(w/\lambda S^2)$.²³ For the paraboloidal profile, the correlation function is paraboloidal near the origin, and the reflectance pattern depends on $(w/\lambda S)$.²³ In the strong diffusion limit, we anticipate $(w/\lambda S^2) \ll 1$ and/or $(w/\lambda S) \ll 1$. This analysis is intended to provide a theoretical guidance for the extremely low reflectance and the flat reflection pattern. However, we realize the limited applicability of the model as the surface profile of our nanotube array consists of interconnected nanotube networks that do not have a well-defined surface-normal even on the submicrometer scale.

We fit the measured reflectance of the nanotube array to the model. For a conical profile, the least-square fit is shown in Figure 4 as the crosses with the fitting parameter, $(w/\lambda S^2) = 0.0046$. For the paraboloidal profile, the fit is shown as the dashed curve with a $(w/\lambda S) = 0.0065$. Both fitting parameters are much less than one, which suggests that our nanotube sample is indeed a strong diffuser. The fitted results predict the low reflectance but not the θ -independent reflection pattern, especially for $|\theta| \geq 45^\circ$. On the other hand, the model yields a good fit to the glassy carbon data shown as purple dots in Figure 4. Furthermore, the deduced fitting parameters are $(w/\lambda S^2) = 0.068$ and $(w/\lambda S) = 0.095$ for the conical and paraboloidal profiles, respectively. These modeling results suggest that the surface profile of our nanotube array may not be easily described by simple scatters. Contrary to typical rough surfaces,^{6,8,9} our nanotube array does not have a continuous surface. It consists of a loosely connected network of nanometer tubes without a well-defined surface-normal either on the sub- λ or on a scale of a few λ 's. The lack of orientation identity to scatter light may be responsible for the θ independence of the reflectance. A comprehensive theoretical understanding is needed to account for the combined effects of the low index of refraction, the strong graphite-like absorption, and random scattering from the unconventional rough surface of the vertically aligned nanotube arrays. We further noted that light absorption could be modified due to light localizations and trapping at the random surface.²⁴ We have also fitted the total reflectance data shown in Figure 3 using the deduced fitting parameters. The fitted results are shown as dashed and solid curves for conical and paraboloidal profiles, respectively. For all cases, the paraboloidal fitting results show a better agreement with experimental data. Again, the model describes the overall trend but predicts a much stronger θ dependence than that observed experimentally.

In summary, we have demonstrated here a new concept based on a low-density nanotube array material that can be engineered to dramatically change an object's index of refraction and nanoscale roughness, hence, its optical reflection. Arrays of vertically aligned carbon nanotubes are shown

to achieve this goal by offering a mechanism for minimizing reflection that is fundamentally different from a traditional antireflection coating or surface roughening. The new degrees of freedom afforded by a nanotube array, such as independent control of tube diameter and tube-to-tube spacing in the 10–50 nanometer range, allow the creation of an extremely low reflectance material. The observed reflectance from the nanotube arrays is the lowest-ever reported reflectance from any material and could have applications ranging from solar energy conversion^{25,26} to pyroelectric detectors.^{13,14}

Acknowledgment. The authors acknowledge preliminary discussions with Dr. Henri Lezec on the absorption measurements. P.M.A. and L.C. acknowledge financial support from focus center New York for Interconnects. S.Y.L. acknowledges financial support from DOE-BES under Grant No. DE-FG02-06ER46347.

References

- (1) Planck, M. *The Theory of Heat Radiation*; Dover Publication, Inc.: New York, 1912.
- (2) Robitaille, P. M. *IEEE Trans. Plasma Sci.* **2003**, *31*, 1263–1267.
- (3) Taft, E. A.; Philipp, H. R. *Phys. Rev.* **1965**, *138*, A197–A202.
- (4) Garcia-Vidal, F. J.; Pitarke, J. M.; Pendry, J. B. *Phys. Rev. Lett.* **1997**, *78*, 4289–4292.
- (5) de Heer, W. A.; Bacsá, W. S.; Chatelain, A.; Gerfin, T.; Humphrey-Baker, R.; Forro, L.; Ugarte, D. *Science* **1995**, *268*, 845–847.
- (6) Kodama, S.; Horiuchi, M.; Kunii, T.; Kuroda, K. *IEEE Trans. Instrum. Meas.* **1990**, *39*, 230–232.
- (7) The Darkest Manmade Substance. *Guinness World Records 2004*; Bantam Doubleday Dell Publishing Group: New York, Toronto, London, Sydney, and Auckland, May 2004; p 242.
- (8) Johnson, C. E. *Met. Finish.* **1980**, *78*, 21–24.
- (9) Brown, R. J. C.; Brewer, P. J.; Milton, M. J. T. *J. Mater. Chem.* **2002**, *12*, 2749–2754.
- (10) Shirley, L. G.; George, N. *Appl. Opt.* **1988**, *27*, 1850–1861.
- (11) Saito, R.; Dresselhaus, G.; Dresselhaus, M. S. *Physical Properties of Carbon Nanotubes*; Imperial College Press: London, 1998.
- (12) Lu, W.; Dong, J.; Li, Z. Y. *Phys. Rev. B* **2000**, *63*, 033401/1–033401/4.
- (13) Theocharous, E.; Deshpande, R.; Dillon, A. C.; Lehman, J. *Appl. Opt.* **2006**, *45*, 1093–1097.
- (14) Lehman, J. H.; Deshpande, R.; Rice, P.; To, B.; Dillon, A. C. *Infrared Phys. Technol.* **2006**, *46*, 246–250.
- (15) (a) Hata, K.; Futaba, D. N.; Mizuno, K.; Namai, T.; Yumura, M.; Iijima, S. *Science* **2004**, *306*, 1362–1364. (b) Yamada, T.; Namai, T.; Haa, K.; Futaba, D. N.; Mizuno, K.; Fan, J.; Yudasaka, M.; Yumura, M.; Iijima, S. *Nat. Nanotechnol.* **2006**, *1*, 131–136.
- (16) Most of the nanotubes were multiwalled, and when the Fe catalyst layer (typically 10 nm of aluminum layer with a 1–5 nm Fe layer on top is used as the active catalyst layer) was down to 1.5 nm, most of them were double-walled. The average diameter of the thin-walled CNTs ranged from 8 to 11 nm, depending on the thickness of the Fe catalyst. The nanotube arrays were very porous, and the density of the nanotube samples ranged between 0.01 and 0.02 g/cm³.
- (17) Williams, M. W.; Arakawa, E. T. *J. Appl. Phys.* **1972**, *43*, 3460–3463.
- (18) Palik, E. D.; Ghosh, G. *The Electronic Handbook of Optical Constants and Thermo-optic Coefficients*, [CD-ROM]; Elsevier Science & Technology Books: Amsterdam, The Netherlands, 1999.
- (19) Nieto-Vesperinas, M. *Opt. Lett.* **1982**, *7*, 165–167.
- (20) O'Donnell, K. A.; Mendez, E. R. *J. Opt. Soc. Am. A* **1987**, *4*, 1194–1205.
- (21) Beckmann, P.; Spizzichino, A. *The Scattering of Electromagnetic Waves from Rough Surfaces*; Artech House: Norwood, MA, 1987.
- (22) Ogilvy, J. A. *Theory of Wave Scattering from Random Rough Surfaces*; Adam Hilger: Bristol, U.K., 1991.

- (23) For the conical type [10], the normalized far-field radiation pattern for a strong diffuser is $\langle I_n \rangle = \cos \theta \frac{2\pi(w/\lambda S)^2}{[\sin^2 \theta - 2 \cos(\phi - \phi_0) \sin \theta \sin \theta_{\text{inc}} + \sin^2 \theta_{\text{inc}}]} \{ 1 + (2\pi w/\lambda S)^2 \times [\sin^2 \theta - 2 \cos(\phi - \phi_0) \sin \theta \sin \theta_{\text{inc}} + \sin^2 \theta_{\text{inc}}] \}^{-3/2}$. For the paraboloidal type [10], the normalized far-field radiation pattern for a strong diffuser is $\langle I_n \rangle = \cos \theta \frac{\pi(w/\lambda S)^2}{[\sin^2 \theta - 2 \cos(\phi - \phi_0) \sin \theta \sin \theta_{\text{inc}} + \sin^2 \theta_{\text{inc}}]} \exp\{ -(\pi w/\lambda S)^2 \times [\sin^2 \theta - 2 \cos(\phi - \phi_0) \sin \theta \sin \theta_{\text{inc}} + \sin^2 \theta_{\text{inc}}] \}$.
- (24) John, S. *Phys. Rev. Lett.* **1984**, 53, 2169–2172.
- (25) *Basic Energy Needs for Solar Energy Utilization*; Basic Energy Science, U.S. Department of Energy: Washington, DC, April 2005; pp 57–73.
- (26) Coutts, T. J.; Guazzoni, G.; Luther, J. *Semicond. Sci. Technol.* **2003**, 18, S144–S150.

NL072369T